1993

Surface Treatment for Mitigation of Hydrogen Absorption and Penetration into AISI 4340 Steel

G. Zheng
University of South Carolina - Columbia

Branko N. Popov
University of South Carolina - Columbia, popov@engr.sc.edu

Ralph E. White
University of South Carolina - Columbia, white@cec.sc.edu

Publication Info

Journal of the Electrochemical Society, 1993, pages 3153-3158.

Surface Treatment for Mitigation of Hydrogen Absorption and Penetration into AISI 4340 Steel

G. Zheng,* B. N. Popov, and R. E. White****

Department of Chemical Engineering, University of South Carolina, Columbia, South Carolina 29208

ABSTRACT

The effectiveness of underpotential deposition of Pb onto a membrane made of AISI 4340 steel on the reduction of the hydrogen evolution reaction on the membrane and the degree of hydrogen ingress into the membrane was determined. In the presence of a monolayer coverage of Pb on the membrane surface, the hydrogen evolution currents were reduced by a factor of two compared with the values obtained on bare steel, and the steady-state hydrogen permeation flux through the steel membranes was reduced by 71%.

The practical use of steel and high strength alloys is limited by cracking hazards due to hydrogen penetration and hydrogen accumulation in the bulk of these alloys.[1,2] Hydrogen embrittlement occurs as a result of hydrogen adsorption on the metal surface followed by diffusion into the crystalline lattice of the substrate. The irreversible accumulation of hydrogen in the bulk of an alloy leads to deterioration of its mechanical properties. In the presence of absorbed hydrogen, changes occur in both the lattice structure and the chemical composition of the alloy. Regardless of the various methods for decreasing hydrogen embrittlement,[3,4] it is difficult to reduce the hydrogen penetration rate into the alloy to a level which provides the elimination of cracking hazards due to hydrogen ingress. A possible solution of this problem is underpotential deposition (UPD) of lead onto the alloy, which should lead to a sharp reduction in the hydrogen ingress.[5]

Juttner[6] found that as a result of UPD of lead and thallium on an iron substrate, the active iron dissolution process as well as the charge-transfer controlled hydrogen evolution are inhibited drastically. The inhibition of the cathodic hydrogen evolution reaction was interpreted as resulting from the lowering of the binding energy of the hydrogen adatoms on Pb and Tl adsorbates.[7,8] The inhibiting action of Pb^{+2} on stress-corrosion-cracking (SCC) of austenitic stainless steels in acidic chloride media has been evaluated by Lafraconi *et al.*[9] Lead ions, even in traces, can exhibit the occurrence of SCC due to the inhibition of the cathodic process of hydrogen evolution. Underpotential deposition of Pb^{+2} was invoked[9] as an explanation of the inhibition of the reaction step involving the adsorption of hydrogen at the alloy surface. Kudryavtsev *et al.*[10] found that the underpotential absorption of zinc onto ARMCO-iron reduces the amount of atomic hydrogen adsorbed into the substrate.

The objective of this work is to estimate the effectiveness of underpotential deposition of lead on the reduction of the hydrogen evolution rate and the degree of hydrogen ingress into AISI 4340 steel.

Experimental

Tafel and linear sweep voltammetry were used to investigate the underpotential deposition of lead on AISI 4340 steel and to determine the diagnostic criteria for the identification of the mechanism of hydrogen discharge in the presence and absence of underpotential deposited lead. The experiments were carried out using stationary AISI 4340 disk electrodes with a geometric area of 0.5 cm^2 placed in an electrolyte containing 0.5*M* $HClO_4$, 0.25*M* $NaClO_4$. Nitrogen was bubbled through the cell and the electrolyte was stirred using a magnetic stirrer. The temperature of the cell was 25°C.

The Devanathan-Stachurski permeation technique[11] was used to investigate both the rate of hydrogen adsorption and hydrogen permeation through a membrane approximately 4 cm^2 made of AISI 4340 steel. The permeation experiments were carried out in a system with two compartments, separated by a bipolar AISI 4340 steel membrane. The current due to hydrogen permeation through the AISI 4340 steel membrane was recorded continuously as a function of time and was measured by setting the potential on the anodic side of the membrane (the side from which the hydrogen emerges) at −0.3 V *vs.* a Hg/HgO reference electrode, a value that corresponds to a practically zero concentration of absorbed atomic hydrogen on the surface.[11] The steel membrane on the cathodic side of the cell was polarized potentiostatically, creating conditions for underpotential deposition and hydrogen evolution. The details of the permeation cell and the auxiliary equipment are given by Subramanyan.[1]

Prior to a permeation experiment, a 0.3 mm thick steel membrane was mechanically polished with 0.3 μm high purity alumina powder to a mirror finish, cleaned in an ultrasonic cleaning bath and saturated with hydrogen in 0.1*N* H_2SO_4 by maintaining for 10 h a cathodic current density of 10 mA/cm^2 on the steel membrane while immersed in 0.1*M* H_2SO_4 in a two-electrode cell. Then, the membrane was removed from the cell and etched for 20 s in a solution containing methyl alcohol and 1% H_2SO_4, rinsed with deionized water, dried in air, and fitted into the permeation cell.

To avoid passivation or dissolution, the anodic side of the membrane was electroplated with a thin layer (0.15 to 0.20 μm) of palladium. The electrodeposition was carried out in an electrolyte containing 2×10^{-5}*M* $Na_2Pd(NO_2)_4$ using a

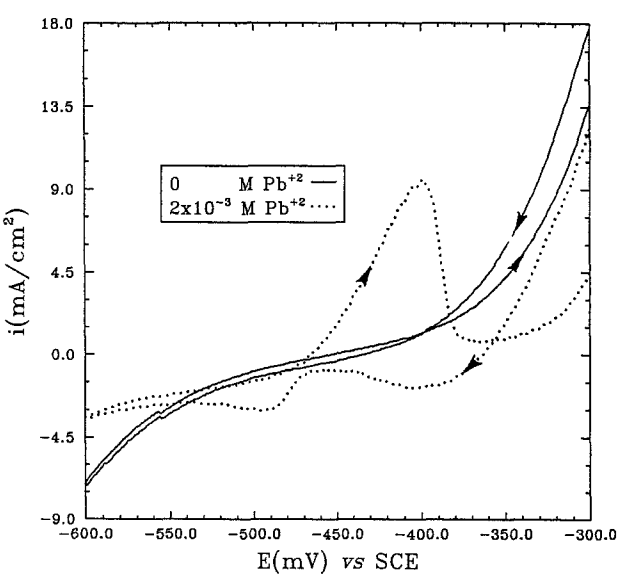

Fig. 1. Potentiodynamic curves obtained on AISI 4340 electrode by using an electrolyte containing 0.5*M* $HClO_4$ and 0.25*M* $NaClO_4$ in the absence and presence of 2×10^{-3}*M* Pb^{+2}, scan rate *v* = 500 mV/s.

* Electrochemical Society Student Member.
** Electrochemical Society Active Member.

current density of 100 μA/cm² for 2 h with the membrane in the permeation cell. Then, the electrolyte was drained off, and the compartment was washed with deionized water and filled with the anodic solution (0.2*M* NaOH). To keep the electrolyte impurities in the lowest possible level, the anodic solution was pre-electrolyzed for at least 24 h in a separate electrolytic cell before putting it in the permeation cell. The anolyte was kept at −0.3 V *vs.* a Hg/HgO reference electrode until the background current was reduced to below 3 μA/cm². Then, the cathodic compartment was filled with a solution containing 0.5*M* $HClO_4$ and 0.25*M* $NaClO_4$, pH 0.3. Prepurified nitrogen was bubbled through both compartments in order to keep them free of oxygen.

Results and Discussion

Cyclic voltammetry studies.—Cyclic voltammetry was used to study the nature of lead deposition on AISI-4340 steel from the electrolyte. The potentiodynamic curves obtained for the hydrogen evolution rate in the supporting electrolyte in the absence and presence of $2 \times 10^{-3}M$ of lead ions are given in Fig. 1. The curve for no lead ions is relatively simple, as expected. However, for the case with lead ions present in the electrolyte, two well-defined cathodic peaks are observed. The first peak occurs at −0.40 V (SCE) and is more noble than the Nernst potential of a lead electrode, [E_{rev} = −0.368 + 0.029 log (2×10^{-3}) = −0.448 V (SCE)]. The second peak is at −0.490 V (SCE) and corresponds to lead deposition from the bulk of the electrolyte. The underpotential shift obtained from the experimental data is, therefore, 0.09 V. In the anodic direction a stripping peak at −0.4 V (SCE) is obtained and corresponds to dissolution of the bulk-deposited lead. The cathodic peak in Fig. 1 at −0.4 V (SCE) indicates that an adsorption process occurs on the AISI 4340 steel with a peak current corresponding to the underpotential deposition of lead. The amount of charge used to deposit lead is determined by integrating the area under the adsorption current peak and is 420 μC/cm². A monolayer coverage of lead adatoms requires a charge of 302 μC/cm² with a roughness factor of 1.[12] The amount of charge of the deposited lead monolayer gives a reasonable roughness factor of 1.4. The roughness factor could vary from 1.4 for a well-polished surface to 12 for an unpolished surface.[13,14]

Polarization measurements-potentiodynamic studies.—Polarization studies were carried out using AISI 4340 steel electrodes with an area of 0.5 cm² in the absence and presence of different concentrations of Pb^{+2} in an electrolyte containing 0.5*M* $HClO_4$ and 0.25*M* $NaClO_4$, pH 0.3. The electrodes were held at −0.45 V (SCE) for 5 min to ensure the lead deposition on the electrode surface. Figure 2 shows Tafel curves obtained using a sweep rate of 1 mV/s for different concentrations of lead. In the absence of lead, a linear region with a Tafel slope of 115 mV with α_c = 0.51 was obtained indicating activation control of hydrogen evolution reaction (HER) in the potential range of −0.47 V (SCE) to −0.620 V (SCE). The presence of lead ions at $10^{-4}M$ in the electrolyte inhibited the HER with a Tafel slope of 130 mV and α_c = 0.45. As the concentration of lead ions was increased above $2 \times 10^{-4}M$, one does not observe any significant change in the Tafel curves indicating that the process is mainly controlled by the surface activity and the crystallographic structure of the substrate and that surface saturation of hydrogen has been completed. As shown in Fig. 3, the hydrogen evolution current, measured at −0.58 V (SCE) on previously underpotential deposited lead decreases from −1.9 mA/cm² (value measured on bare steel in supporting electrolyte) to −1.06 mA/cm². The polarization experiments carried out in the presence of lead in the electrolyte indicate that the underpotential deposited lead inhibits the adsorption step in the hydrogen evolution reaction which results in an increase of the HER overpotential and, consequently, a decrease of the current density.

To determine the diagnostic criteria for the identification of the mechanism of the discharge of hydrogen ions on AISI 4340 steel, separate experiments were carried out with the

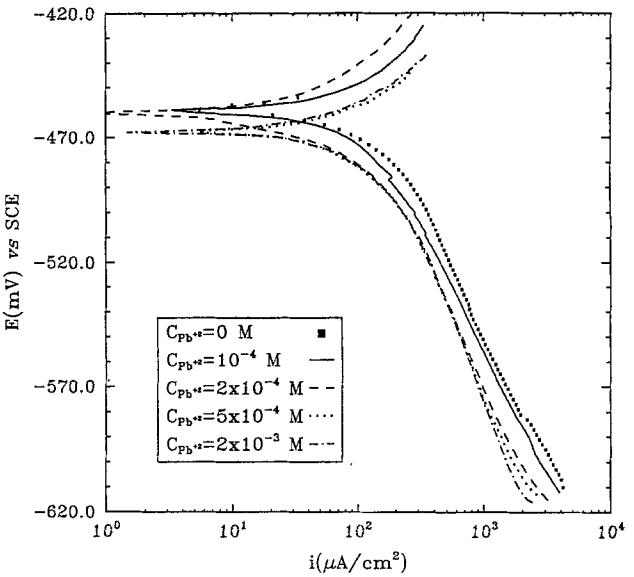

Fig. 2. Cathodic polarization curves obtained on AISI 4340 steel by using an electrolyte containing 0.5*M* $HClO_4$ and 0.25*M* $NaClO_4$ in the absence and in the presence of different concentrations of Pb^{+2}. The underpotential deposition was carried out at *E* = −0.45 V (SCE) for 5 min. Scan rate, *v* = 1 mV/s.

supporting electrolyte in which the cathodic current density was measured as a function of the applied overpotential. In these experiments, the alloy membrane on the cathodic side of the cell was polarized potentiostatically. The current-potential relationship is presented in Fig. 4, where two different slopes are observed. At low overpotentials the slope $-\partial\eta/\partial \log i_c$ is 118 mV/decade which corresponds to $2.3 \times 2RT/F$ (298.15 K). This is a diagnostic criteria indicating that the mechanism of the hydrogen evolution reaction is coupled discharge-recombination with Langmuir isotherm for hydrogen coverage.[1]

At higher overpotentials, the current *vs.* potential plot gives a slope of 177 mV/decade, which corresponds to $2.3 \times 3RT/F$ (T = 298.15 K). This indicates that the HER has the same mechanism but with Temkin isotherm of hydrogen coverage.[1] The transfer coefficients calculated by using these two sets of data are 0.52 and 0.50, respectively. A value of 0.51 for the transfer coefficient is used in all calculations.

Hydrogen permeation studies.—In the permeation experiments, the hydrogen permeation transients through an AISI 4340 steel membrane with a thickness of 0.30 mm were obtained in supporting electrolyte containing 0.5*M* $HClO_4$ and 0.25*M* $NaClO_4$ in the absence of lead. The atomic

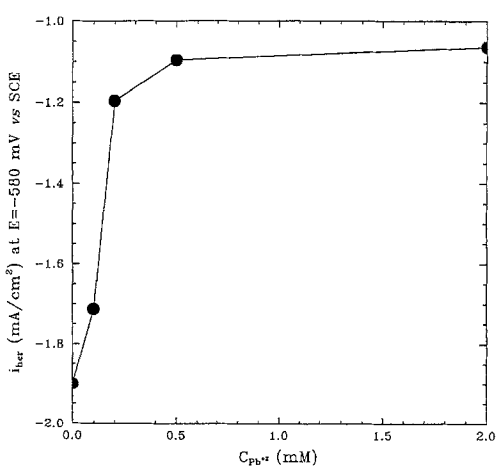

Fig. 3. The hydrogen evolution current density estimated at *E* = −0.58 V (SCE) as a function of Pb^{+2} concentration.

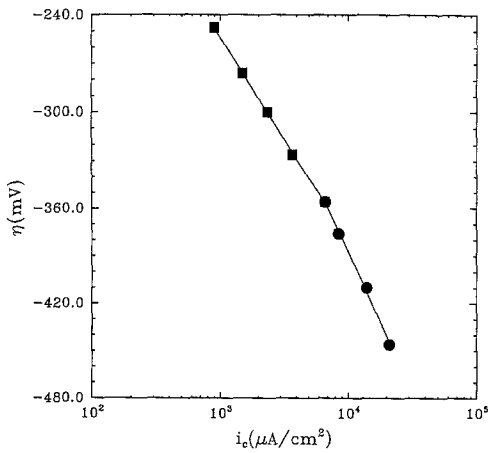

Fig. 4. Cathodic current-overpotential relationship for hydrogen evolution reaction obtained on AISI 4340 steel membrane in an electrolyte containing 0.5*M* $HClO_4$ and 0.25*M* $NaClO_4$ (pH 0.3).

hydrogen permeation current densities *vs.* time for different cathodic potentials are plotted in Fig. 5. As seen in Fig. 5, the steady-state hydrogen permeation current increases with the increase of the applied cathodic potential until the cathodic potential reaches a value of −0.600 V (SCE). Above this potential, the steady-state hydrogen permeation current is independent of the applied potential. Similar complex behavior of the hydrogen permeation transients has been observed in the past.[15,16] This phenomena is probably due to the hydrogen surface saturation or to an activation of trapping sites of the substrate structure at high overpotentials. The diffusivity of atomic hydrogen through the AISI 4340 steel membrane was evaluated by using the equation[17] $t_{1/2} = 0.138L^2/D$, where L is the membrane thickness, D is the hydrogen diffusivity, and $t_{1/2}$ is time corresponding to half-rise of the permeation curve. For L = 0.3 mm and $t_{1/2}$ = 426 s [a value obtained for the permeation curve E_c = −0.60 V (SCE) presented in Fig. 5], the diffusivity of atomic hydrogen was calculated to be 2.9×10^{-7} cm^2/s.

When carrying out the experiments with a bipolar membrane, the steady-state rate of hydrogen penetration in a diffusion mode can be presented by the following equations obtained for two typical boundary conditions:

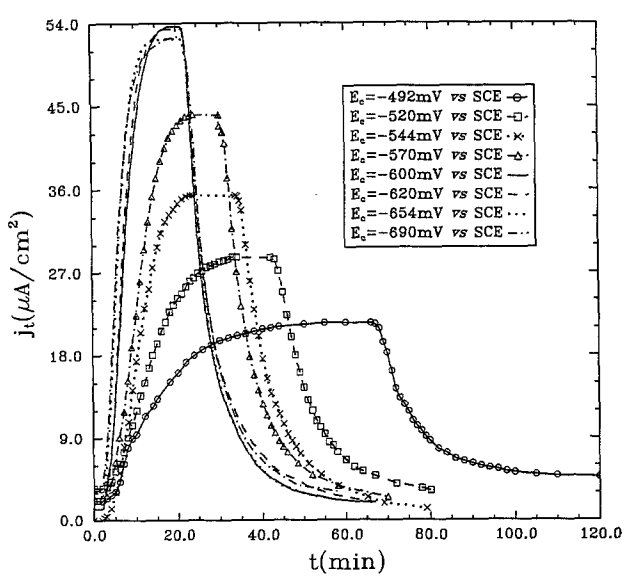

Fig. 5. The atomic hydrogen permeation transients through AISI 4340 membrane as a function of time for different applied cathodic potentials in an electrolyte containing 0.5*M* $HClO_4$ and 0.25*M* $NaClO_4$ (pH 0.3), the membrane thickness = 0.30 mm.

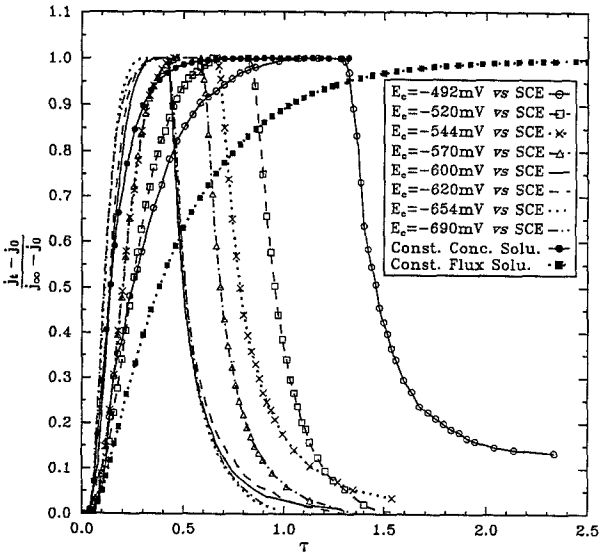

Fig. 6. The comparison of the experimental results given in Fig. 5 with the theoretical solutions for the two typical theoretical solutions in dimensionless forms.

1. for the case where the hydrogen concentration at the entry side of the membrane is constant[18]

$$\frac{j_t - j_o}{j_\infty - j_o} = 1 + 2\sum_{n=1}^{\infty}(-1)^n \exp(-n^2\pi^2\tau) \qquad [1]$$

2. for the case where the flux of the hydrogen entering the membrane is constant[19]

$$\frac{j_t - j_o}{j_\infty - j_o} = 1 - \frac{4}{\pi}\sum_{n=0}^{\infty}\frac{(-1)^n}{(2n+1)}\exp\left\{-\frac{(2n+1)^2\pi^2\tau}{4}\right\} \qquad [2]$$

where j_t is transient hydrogen permeation current density, j_o is initial hydrogen permeation current density (may or may not be zero), j_∞ is steady-state hydrogen permeation current density, $\tau = tD/L^2$, where t is time. The experimental permeation curves in dimensionless form are compared with the two theoretical solutions for hydrogen permeation in Fig. 6. According to Fig. 6, at high cathodic potentials, the experimental permeation curves are close to the theoretical curve obtained where the boundary condition is a constant hydrogen concentration at the entry side of the membrane. At lower applied cathodic potentials as seen in

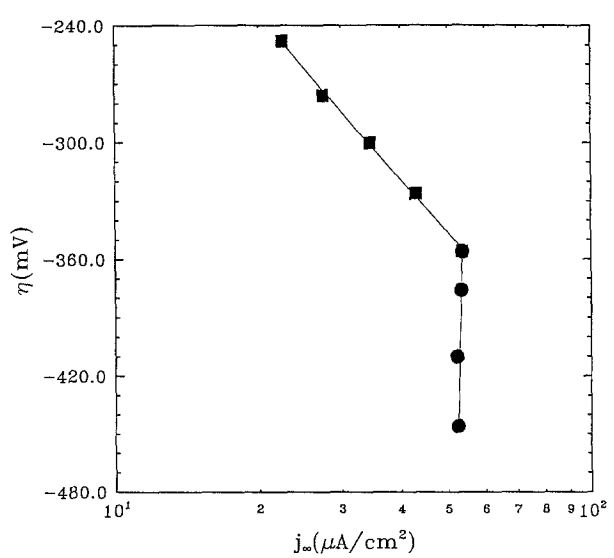

Fig. 7. Hydrogen permeation current-overpotential dependence obtained on AISI 4340 steel membrane in an electrolyte containing 0.5*M* $HClO_4$ and 0.25*M* $NaClO_4$ (pH 0.3), and the membrane thickness = 0.30 mm.

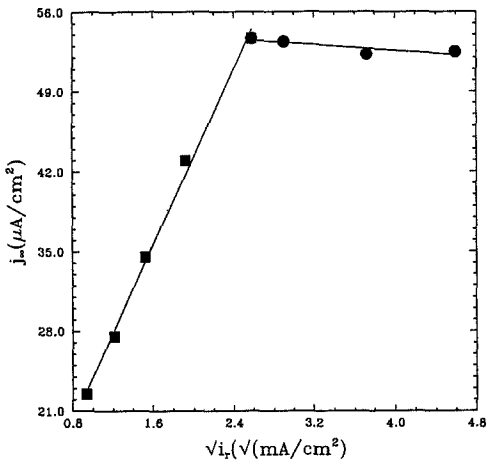

Fig. 8. Plot of hydrogen permeation current vs. square root of the hydrogen recombination current density in an electrolyte containing 0.5*M* $HClO_4$ and 0.25*M* $NaClO_4$ at pH 0.3, and the membrane thickness = 0.3 mm.

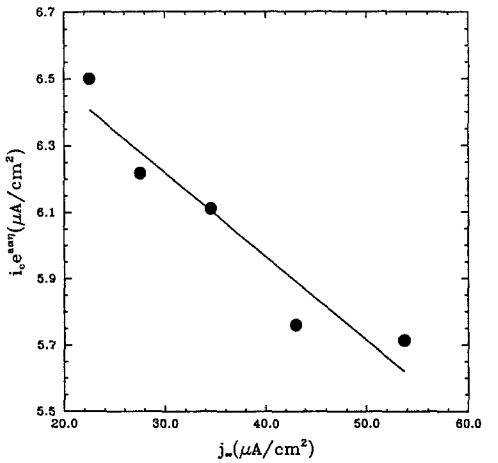

Fig. 9. Plot of $i_c e^{\alpha\alpha\eta}$ as a function of hydrogen permeation through an AISI 4340 steel membrane in an electrolyte containing 0.5*M* $HClO_4$ and 0.25*M* $NaClO_4$ (pH 0.3), and the membrane thickness = 0.30 mm.

Fig. 6, the experimental permeation transients are approaching the theoretical curve obtained by using boundary conditions in which the flux of the hydrogen entering the membrane is constant.

Figure 7 shows the dependence of the steady-state hydrogen permeation current upon the overpotential. This plot also provides a diagnostic criteria for the identification of the mechanism of the discharge of hydrogen ions on the steel membrane. At lower overpotentials the slope $-\partial\eta/\partial \log j_\infty = 273$ mV/decade $\approx 2.3 \times 4RT/F$ ($T = 298.15$ K) which indicates a coupled discharge-recombination mechanism.[1] At higher overpotentials the permeation criteria does not apply due to the fact that j_∞ is independent of η.

Using the mechanistic model developed by Iyer *et al.*,[20] the hydrogen surface coverage and the surface concentration, the hydrogen absorption, discharge, and recombination rate constants as well as the HER coverage-dependent transfer coefficient, α, and the exchange current density i_o were computed from a knowledge of the steady-state hydrogen permeation current, cathodic charging current, hydrogen diffusivity, and hydrogen overvoltage. This was done by assuming that (*i*) the recombination step of hydrogen is not rate-determining so that the hydrogen atom oxidation can be neglected ($\eta >> RT/F$); (*ii*) the Langmuir isotherm is used to describe the hydrogen coverage of the substrate; (*iii*) the intermediate hydrogen adsorption-absorption reaction is in local equilibrium; and (*iv*) the hydrogen permeation process is described by a simple diffusion model through the membrane. With this assumptions, one can derive the following relationships[20]

$$i_r = Fk_3\theta_H^2 \quad [3]$$

$$j_\infty = \frac{k''\theta_H}{b} \quad [4]$$

$$j_\infty = \frac{k''}{b\sqrt{Fk_3}}\sqrt{i_r} \quad [5]$$

$$i_c e^{\alpha\alpha\eta} = -\frac{bi_o'}{k''} j_\infty + i_o' \quad [6]$$

where $i_r = i_c - j_\infty$ is the hydrogen recombination current density, i_c is the cathodic current density, $b = L/FD$, L is the membrane thickness, F is the Faraday constant, D is hydrogen diffusion coefficient, $a = F/RT$, α is the transfer coefficient, η is the overpotential, R is the gas constant, T is the temperature, and θ_H is the hydrogen surface coverage, k_3 is the recombination rate constant, k'' is the thickness dependent adsorption-absorption constant, $i_o' = i_o/1 - \theta_e$, here i_o is the exchange current density, and θ_e is equilibrium hydrogen coverage.

Figure 8 shows the dependence of the steady-state permeation current upon the square root of the recombination current density. A linear relationship is obtained at lower overpotentials which is consistent with Eq. 5. In Fig. 9, $i_c e^{\alpha\alpha\eta}$ is plotted *vs.* j_∞. Using the slopes and intercepts in Fig. 8 and 9 and Eq. 5 and 6, the values of i_o', k'', and k_e were computed to be 7.2×10^{-6} A/cm^2, 4.1×10^{-4} mol/cm^3, and 1.1×10^{-6} mol/cm^2 s, respectively. Substituting this calculated value of k_3 and the experimentally measured $i_r = i_c - j_\infty$ into Eq. 3, the hydrogen surface coverage was calculated and is presented in Fig. 10 as a function of the hydrogen overpotential.

As stated earlier, lead adatoms cause a suppression of hydrogen adsorption by chemically changing the substrate surface. As a consequence, the hydrogen adsorption process is altered without changing the mechanical or physical properties of the substrate. According to Eq. 4, the hydrogen permeation flux may be reduced due to: (*i*) decreasing the hydrogen surface coverage or (*ii*) decreasing the absorption-adsorption constant (k'').

To determine if any inhibition of the hydrogen permeation current occurs in the presence of lead on the surface, the hydrogen permeation through AISI 4340 steel membrane with a thickness of 0.45 mm was studied in the presence of underpotential deposited lead on the surface in supporting electrolyte containing 0.5*M* $HClO_4$ and 0.25*M* $NaClO_4$. To avoid the bulk deposition of lead on the steel substrate, an underpotential deposition of Pb^{+2} was ensured by predepositing the substrate, according to our potentiodynamic studies using an electrolyte containing $2 \times 10^{-3}M$ Pb^{+2} at -0.45 V (SCE). The prepurified nitrogen was

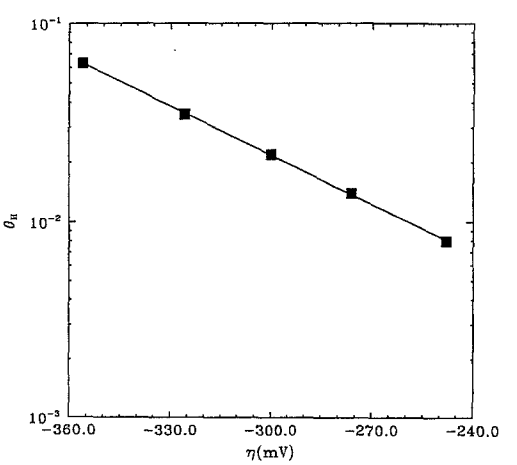

Fig. 10. Plot of hydrogen coverage as a function of the overpotential on AISI 4340 membrane in an electrolyte containing 0.5*M* $HClO_4$ and 0.25*M* $NaClO_4$ (pH 0.3).

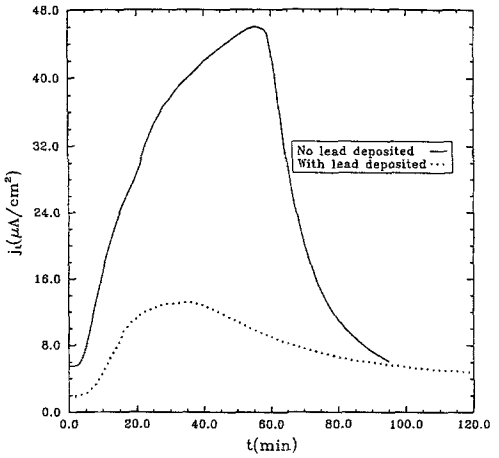

Fig. 11. Hydrogen permeation transients through an AISI 4340 steel membrane at $E = -0.6$ V (SCE) in the absence and presence of underpotential deposited lead. $C_{Pb^{2+}} = 2 \times 10^{-3} M$, membrane thickness = 0.45 mm.

continuously passed through the cell during the deposition and later during the permeation experiment to avoid the oxidation of the substrate or deposited material. In order to eliminate any possible influence of PbH_2 on hydrogen permeation studies, one should also avoid the formation of lead hydride on steel. Thus, the permeation studies were carried out at −0.6 V (SCE) and −0.7 V (SCE), which are more noble potentials than the deposition potential of lead hydride [−1.53 V (SCE)].[21]

The resulting hydrogen permeation transients obtained at −0.6 and −0.7 V (SCE) are shown in Fig. 11 and 12, respectively. With lead on the steel, the steady-state hydrogen flux at −0.6 V (SCE) was reduced by 71%, while at applied potential of −0.7 V (SCE), the flux was reduced by 67%.

Conclusion

Hydrogen cathodic current density was measured potentiostatically as a function of the applied overpotential to determine the diagnostic criteria for the identification of the mechanism of the discharge of hydrogen ions on AISI 4340 steel. At low overpotentials, the Tafel slope is 118 mV/decade. This corresponds to $2.3 \times 2\ RT/F$, indicating that the mechanism of the hydrogen evolution reaction is coupled discharge-recombination with Langmuir isotherm for hydrogen coverage. At a higher overpotential, the current *vs.* potential plot gives a slope of 177 mV/decade, which corresponds to $2.3 \times 3\ RT/F$. This indicates that HER has the same mechanism but with the Temkin isotherm for hydrogen coverage. A plot of the steady-state hydrogen permeation current *vs.* the overpotential gives a slope which corresponds to $2.3 \times 4\ RT/F$, which confirms the coupled discharge-recombination mechanism for hydrogen discharge at low overpotentials.

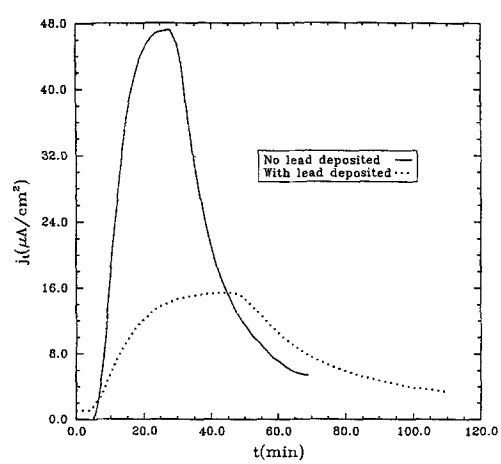

Fig. 12. Hydrogen permeation transients through an AISI 4340 steel membrane at $E = -0.710$ V (SCE) in the absence and presence of underpotential deposited lead. $C_{Pb^{2+}} = 2 \times 10^{-3} M$, membrane thickness = 0.45 mm.

The hydrogen surface coverage, the hydrogen absorption-adsorption constant, recombination rate constant, transfer coefficient, as well as the exchange current density were computed from a knowledge of the steady-state hydrogen permeation current, cathodic charging current, hydrogen diffusivity, and hydrogen overvoltage. An underpotential deposited lead onto the AISI steel reduces the steady-state hydrogen flux by 71%.

Acknowledgment

Technical assistance and financial support by A. John Sedriks, the Office of Naval Research, under Contract No. N00014-92-J-1434 are gratefully acknowledged.

Manuscript submitted April 1, 1993; revised manuscript received Aug. 9, 1993.

The University of South Carolina assisted in meeting the publication costs of this article.

LIST OF SYMBOLS

a	F/RT, a constant, V^{-1}
b	$L/(FD)$ a constant, $(A\ cm)^{-1}$
$C_{Pb^{+2}}$	lead concentration, mol cm^{-3}
D	hydrogen diffusion coefficient, $cm^2\ s^{-1}$
E_{app}	applied potential, V
E^{eq}	equilibrium potential for the HER, V
E_c	cathodic potential, V
F	Faraday constant, 96,487 C/eq
i	current density, A/cm^2
i_c	cathodic current density, A/cm^2
i_{HER}	hydrogen evolution reaction current density, A/cm^2
i_r	hydrogen recombination current density, A/cm^2
i_o	exchange current density, A/cm^2
i_o'	$i_o/1 - \theta_e$, A/cm^2
j_t	transition hydrogen permeation current density, A/cm^2
j_o	initial hydrogen permeation current density, A/cm^2
j_∞	steady-state hydrogen permeation current density, A/cm^2
k_3	recombination rate constant, mol $(cm^2\ s)^{-1}$
k''	thickness dependent absorption-adsorption constant, mol cm^{-3}
L	membrane thickness, cm
R	gas constant, 8.3143 J $(mol\ K)^{-1}$
t	time, s
T	temperature, K
v	scan rate, mV/s

Greek

α	transfer coefficient, dimensionless
α_c	cathodic transfer coefficient, dimensionless
θ_e	equilibrium hydrogen surface coverage, dimensionless
θ_H	hydrogen surface coverage, dimensionless
η	overpotential, $[E_{app} - E^{eq}]$, V
τ	$t\ D/L^2$, dimensionless time

REFERENCES

1. P. Subramanyan, in *Comprehensive Treatise of Electrochemistry*, Vol. 4, J. O'M. Bockris, B. E. Conway, E. A. Yeager, and R. E. White, Editors, p. 411, Plenum Press, Inc., New York (1981).
2. S. Bagaev, K. Pedan, and V. Kudrjavtsev, *Zatshtita Metallov*, **19**, 968 (1983).
3. V. Kudryatsev, K. Pedan, H. Barbashkina, and S. Vagramjan, *ibid.*, **9**, 161 (1973).
4. J. J. Reilly, *Z. Phys. Chem.*, **117**, 655 (1979).
5. D. M. Kolb, M. Przasnyski, and H. Gerisher, *J. Electroanal. Chem.*, **54**, 25 (1974).
6. K. Jüttner, *Werkst. Korros.*, **31**, 358 (1980).
7. A. M. Abd El Halim, K. Jüttner, and W. J. Lorenz, *J. Electroanal. Chem.*, **106**, 193 (1980).
8. N. Faruya and S. Moto, *ibid.*, **70**, 165 (1976).
9. G. Lafraconi, F. Mazza, E. Sivieri, and S. Torchio, *Corros. Sci.*, **18**, 617 (1978).
10. V. Kudryavtsev, K. Pedan, and S. Bagaev, *J. Electroanal. Chem.*, **248**, 421 (1988).
11. M. A. V. Devanathan and L. Strachurski, *Proc. R. Soc.*

London, Ser., A, **270,** 90 (1962).
12. A. Bewick and B. Thomas, *J. Electroanal. Chem.,* **84,** 127 (1977).
13. S. H. Cadle and S. Bruckenstein, *This Journal,* **119,** 1166 (1972).
14. I. Fried and H. Barak, *J. Electroanal. Chem.,* **30,** 279 (1971).
15. W. Raczynski, *Archiwum Hutnictwa,* **3,** 59 (1958).
16. T. Zakroczymski, Z. Szklarska-Smialowska, and M. Smialowski, *Werkst. Korros.,* **26,** 617 (1975).
17. B. S. Chaudhari and T. P. Radhakrishnan, *Corros. Sci.,* **30,** 12, 1219 (1990).
18. M. A. V. Devanathan, Tech. Rep. ONR/551/22/NR-036-028, Office of Naval Research, Washington, DC (1961).
19. N. Boes and H. Zuchner, *J. Less-Common Metals,* **49,** 223 (1976).
20. R. N. Iyer, H. W. Pickering, and M. Zamanzadeh, *This Journal,* **136,** 2463 (1989).
21. M. Pourbaix, *Atlas of Electrochemical Equilibria in Aqueous Solution,* Pergamon Press and Ceberlcor, Brussels (1966).

The Role of the Residual Solvent for Chemical Amplification Resists

Tsukasa Azuma,[a] Hiromi Niiyama, Hideyuki Sasaki,[b] and Ichiro Mori

ULSI Research Laboratory and [b]Environmental Engineering Laboratory, Toshiba Corporation, 1, Komukai Toshiba-cho, Saiwai-ku, Kawasaki 210, Japan

ABSTRACT

The role of the residual solvent for chemical amplification resists has been investigated. The validity of a model that the mobility of the acid catalyst is governed by the residual solvent assumed to act as a reaction medium is discussed. It has been found that the optimization of the prebake conditions can provide a high resolution without sacrificing the sensitivity. The change in the residual solvent content which is fixed by the prebake conditions has also been found to be a reversible process from the experimental results of a solvent vapor treatment. The optimum post-exposure bake (PEB) conditions which govern the lithographic properties of the resist can be concluded to be strongly dependent on the residual solvent content of the resist film.

In the past few years, chemical amplification resists based on acid catalyzed reactions have been broadly utilized in the development of advanced lithography.[1] However, the lack of fundamental understanding of the mechanisms of these resist systems prevented the development of stable processing conditions in spite of their reactions that are different from conventional imaging mechanisms. In a chemical amplification scheme, an acid generated species induced by exposure is considered to catalyze many chemical events ranging from diffusion by means of the thermal energy provided during post-exposure bake (PEB).[2] Therefore, it can be expected that the acid catalyzed reactions are greatly affected by the PEB conditions.

On the other hand, it was reported that there exist strong influences of prebake and PEB conditions not only on the sensitivity but also on the resolution capability of chemical amplification resists.[3,4] These results indicate that the diffusion range of the acid catalyst must play a very crucial role in the resist performance.[5,6] The authors have found that the lithographic properties of the resist were dependent on the residual solvent content which was fixed by the prebake conditions during process optimization experiments leading towards quarter-micron lithography by an electron-beam single-layer resist system.[7] Furthermore, these tendencies were remarkable in fine resist patterns such as 0.25 μm lines/spaces when thick resist films such as 1 μm in thickness were used. The authors' proposed model assumed that the residual solvent of the resist film can affect the diffusion length of the acid catalyst. This is because it is thought to act as a reaction medium.

In this paper, the role of the residual solvent for chemical amplification resists is discussed, using a novolak-based chemically amplified negative-type electron-beam resist SAL601 made by Shipley Co., aiming at a deeper understanding of the mechanisms of these resist systems.

[a] Present address: Toshiba/IBM/Siemens 256MDRAM Development Project, Toshiba America Electronic Components Inc., IBM East Fishkill Facility 33A, Hopewell Junction, NY 12533.

Experimental

The SAL601 resist was spin-coated onto silicon wafers 1 μm thick after hexamethyldisilazane (HMDS) vapor treatment at 23°C for 270 s. The wafers were then prebaked on a hotplate at 85, 125, and 135°C for 60 s.

The validity of the authors' proposed model was experimentally examined for the resist films by carrying out ethylcellosolve acetate (ECA), which is the primary component of the solvent, vapor treatment. The experimental apparatus is illustrated in Fig. 1. Both wafers previously prebaked at 85 and 125°C, respectively, were placed on a supporter at 23°C for 30 min above ECA in a closed laboratory dish, and then they were prebaked again at 85 or 125°C, respectively.

Exposure was carried out on an EX-7, vector-scan variable-shaped beam direct writing machine, at 40 kV with a current density of 60 A/cm^2. After exposure, the wafers were given a PEB on a hotplate at 115, 120, and 125°C for 120 s for each prebake condition, except at 115°C for 120 s for the samples after the solvent vapor treatment, and then developed in a 0.36*N* tetramethylammonium hydroxide (TMAH) aqueous solution at 23°C for 6 min.

The resist patterns were observed using scanning electron microscopy (SEM). The resist film was analyzed by Fourier-transform infrared (FT-IR) spectroscopy to monitor the change in the residual solvent content of the resist film. Reflection-absorption spectroscopy in the FT-IR measurements were applied.

Results and Discussion

Figure 2 shows the resist patterns of 0.5 μm lines/spaces with respect to both prebake and PEB temperatures. Variations in the resist patterns with respect to both prebake and PEB temperatures which were identical with those for Fig. 2 are shown in Fig. 3 for 0.25 μm lines/spaces. All patterns were able to be successfully delineated, as shown in Fig. 2. There is little difference in resolution for all combinations of the prebake and PEB temperatures. However, 0.25 μm line/space patterns where the prebake temperature was 85°C or where the PEB temperature was 125°C